A 3D simulation of drifting snow in the turbulent boundary layer

Huang Ning[1,2], Zhengshi Wang[1,2*]

[1]Key Laboratory of Mechanics on Disaster and Environment in Western China (Lanzhou University), The Ministry of Education of China, 730000

[2]Department of Mechanics, School of Civil Engineering and Mechanics, Lanzhou University, Lanzhou, 730000, China

[*] *Correspondence to*: Zhengshi Wang (Email: wangzhsh2013@lzu.edu.cn)

Abstract. The drifting snow is one of the most important factors that affect the global ice mass balance and hydrological balance. Current models of drifting snow are usually one- or two-dimensional, focusing on the macroscopic quantities of drifting snow under temporal average flow. In this paper, we take the coupling effects between wind and snow particles into account and present a 3-D model of drifting snow with mixed grain size in the turbulent boundary layer. The Large Eddy Simulation (LES) method is used for simulating the turbulent boundary layer of the wind field and the 3-D trajectory of every motion snow particle is calculated through Lagrangian Particle Tracking method. Both simulation and experimental results agree well. The results indicated that the motion trajectories of snow particles, especially the small snow particles, are obviously affected by the turbulent fluctuation and turbulent kinetic energy (TKE) is obvious enhanced by drifting snow. The visualized observation of drifting snow in the turbulent boundary layer demonstrates apparent 3-D structure and snow streamers, which lead to an intermittent transport of the snow particles and spatial inhomogeneity. The macro statistics of drifting snow indicates that the variation of spanwise velocity of snow particles along height depends on the friction velocity and is one order smaller than that of streamwise velocity.

1 Introduction

The phenomenon of the loose snow particles traveling near the land surface under the action of wind is known as drifting snow. As a typical two-phase flow, drifting snow is widely distributed in the globe and has significant impacts on the natural environment and the social economy. On one hand, drifting snow is one of the main causes of the temporal and spatial variation of snow distribution, contributes greatly to the mass balance of the ice sheets (Gallée et al., 2013), and further affects global climate system. The seasonal snow cover also deeply affects the hydrological balance in cold regions, thus is of glaciological and hydrological importance. On the other hand, drifting snow causes snow accumulation on the road and reduces visibility, which may seriously affect the traffic and human activities, and its resultant non-uniform distribution of snow layer may induce and aggravate various natural disasters, such as flood, avalanche, mudslides and landslide (Michaux et al., 2001). These disasters may result in not only huge direct and indirect economic losses, but also human casualties. Thus, in-depth study on the drifting snow is considered to be essential to comprehensively understanding the ice mass balance and hydrological balance.

The transport processes of snow grains have been extensively investigated (Pomeroy et al., 1993; Clifton and Lehning, 2008). Many models were proposed by taking the snow particles as continuous phase (Uematsu et al., 1991; Mann, 2000; Taylor, 1998; Déry and Yau, 1999; Fukushima et al., 1999, 2001; Xiao et al., 2000; Bintanja, 2000a, 2000b). These models have a significant role in promoting the drifting snow research although some information can not be acquired from these models, for example, the trajectory of particle and its movement mechanisms. Subsequently, Nemoto and Nishimura (2004) studied the snow drifting process based on particle tracking in a turbulent boundary layer and their 1-D model included four sub-processes: the aerodynamic entrainment of snow grains, grain-bed collision, grain trajectories and wind modification. Later, Zhang and Huang (2008) presented a steady state snow drift model combined with the initial velocity distribution function and analyzed the structure of drifting snow at steady state. However, neither the details of the spatial variation of snow drifting nor the whole turbulent structure of wind field can be described due to limitation of their models. 3-D simulation of drifting snow gradually carried out in recent years. Gauer (2001) first simulated the blowing and drifting snow in Alpine terrain with Reynolds Averaged Navier-Stokes (RANS) approaches. Also, Schneiderbauer and Prokop (2011) developed the SnowDrift3D model based on RANS. Vionnet et al. (2014) went on a study of large-scale erosion and deposition using a fully coupled snowpack/atmosphere model. Groot et al. (2014) simulated the small-scale drifting snow with a Lagrangian stochastic model based on LES and the intermittency of drifting snow was analyzed. And snow particles were uniform size in most previous models, which is different from the natural situation. To date, a comprehensive study on drifting snow in the turbulent field is indispensable for a thorough understanding of the complex drifting snow.

In this paper, based on the model of Dupont et al. (2013) that developed for blown sand movement, the Advanced Regional Prediction System (ARPS, version 5.3.3), which is a middle-scale meteorological model, is applied in a small-scale for drifting snow and a series of adaptations are made for drifting snow simulation. We performed a numerical study of drifting snow in the turbulent boundary layer by taking the 3-D motion trajectory of snow particles with mixed grain size, the grain-bed interaction, and the coupling effect between snow particles and wind field into consideration and used it to directly calculate the velocity and position of every single snow particle in turbulent atmosphere boundary layer, the transport rate and velocity distribution characteristics of drifting snow, and the mean particles size at different heights. The paper is structured as follows: Section 2 briefly introduces the model and methods; Section 3 illuminates the model validations; Section 4 presents the simulation results and discussions, and Section 5 is the conclusion.

2 Model and Methods

2.1 Turbulent boundary layer

The ARPS developed by University of Oklahoma is a three-dimensional, non-hydrostatic, compressible LES model and has been used for simulating wind soil erosion (Vinkovic et al., 2006; Dupont et al., 2013). In this paper, it is used for modeling the drifting snow.

Snow saltation movement in the air is a typical two-phase movement, in which the coupling of particles and the wind field is a key issue. Vinkovic et al. (2006) introduced the volume force caused by the particles into Navier-Stokes equation of ARPS and The conservation equations of momentum and subgrid scale (SGS) turbulent kinetic energy (TKE) after filtering can be expressed as (Vinkovic et al., 2006; Dupont et al., 2013):

$$\frac{\partial \tilde{u}_i}{\partial t}+\tilde{u}_j\frac{\partial u_i}{\partial x_j}=-\frac{1}{\overline{\rho}}\frac{\partial}{\partial x_i}\left(\tilde{p}''-\alpha_{div}\frac{\partial \overline{\rho}\tilde{u}_j}{\partial x_i}\right)-g\left(\frac{\tilde{\theta}''}{\overline{\theta}}-\frac{c_p}{c_v}\frac{\tilde{p}''}{\overline{p}}\right)\delta_{i3}-\frac{\partial \tau_{ij}}{\partial x_j}-f_i \tag{1}$$

$$\begin{aligned}\frac{\partial e}{\partial t}+\tilde{u}_j\frac{\partial e}{\partial x_j}=&-\tau_{ij}\frac{\partial \tilde{u}_i}{\partial x_j}+\frac{\partial}{\partial x_j}\left(2\left(\left(1-\delta_{j3}\right)\nu_{th}+\delta_{j3}\nu_{tv}\right)\frac{\partial e}{\partial x_j}\right)\\&-\frac{g}{\overline{\theta}}\tau_{3\theta}-\varepsilon-\frac{1}{V_{grid}}\sum_{s=1}^{N_p}\frac{m_p}{\overline{\rho}}\frac{2e}{T_P+T_L}f\left(Re_p\right)\end{aligned} \tag{2}$$

where the tilde symbol indicates the filtered variables and the line symbol represents grid volume-averaged variables. $x_i\,(i=1,2,3)$ stand for the streamwise, lateral, and vertical directions, respectively, u_i refers to the instantaneous velocity component of three directions, δ_{ij} is the Kronecker symbol, α_{div} means the damping coefficient, p and ρ are the pressure and density of air, respectively; g is the gravity acceleration, θ indicates the potential temperature, c_p and c_v are the specific heat of air at constant pressure and volume, respectively; t is time, τ_{ij} denotes the subgrid stress tensor, and f_i is the drag force caused by the particles and can be written as (Yamamoto et al., 2001):

$$f_i=\frac{1}{\rho V_{grid}}\sum_{s=1}^{N_p}m_p\frac{u_i(x_p(t),t)-u_{pi}(t)}{T_p}f(Re_p) \tag{3}$$

where V_{grid} is the grid cell volume, N_P stands for the number of particles per grid, m_p means the mass of particles, $u_{pi}(t)$ and $u_i(x_p(t),t)$ represent the velocity of particles and the wind velocity at grain location at time t, respectively, and $f(Re_p)$ is an empirical relation of the particle Reynolds number Re_p (Clift et al., 1978):

$$\begin{aligned}&f(Re_p)=1 && (Re_p<1)\\&f(Re_p)=1+0.15\mathrm{Re}_p^{0.687} && (Re_p\geq 1)\end{aligned} \tag{4}$$

In the equation (2), e is the SGS TKE, ν_{th} and ν_{tv} stand for the horizontal and vertical eddy viscosities, respectively, $\tau_{3\theta}$ is the subgrid heat flux, and ε indicates the dissipation rate of SGS TKE. T_p and T_L represent the particle response time and the Lagrangian correlation timescale, respectively, and can expressed as

$$T_p = \frac{\rho_p d_p^2}{18\rho \nu} \text{ and } T_L = \frac{4e}{3C_0\varepsilon} \quad (5)$$

where C_0 is the Lagrangian constant and ν denotes the molecular kinematic viscosity.

2.2 Governing equation of particle motion

Because snow particles have much higher density ρ_p than air ($\rho_p/\rho \approx 10^3$) and much smaller diameter d_p than Kolmogorov scale, in this simulation, they are approximately regarded as a sphere and only possess gravity and drag force. Thus, their motion governing equation can be expressed as (Vinkovic et al., 2006)

$$\frac{d\vec{x}_p(t)}{dt} = \vec{v}_p(t) \quad (6)$$

$$\frac{d\vec{v}_p(t)}{dt} = \frac{\vec{v}(\vec{x}_p(t),t) - \vec{v}_p(t)}{T_p} f(Re_p) + \vec{g} \quad (7)$$

where $\vec{v}_p(t)$ and $\vec{v}(\vec{x}_p(t),t)$ are the velocity of the particle and the fluid velocity of particle position at time t, respectively.

It is worth noting that the inertia effect of snow particles is considered by evaluating the maximum particle response time, so the particle motion is the dynamical calculation of time step, which is guaranteed to be less than the maximum particle response time.

2.3 Grain-bed interactions

2.3.1 Aerodynamic Entrainment

Snow particles will be entrained into the air if the shear force produced by air flow is large enough. The number of entrainment N (per unit area per unit time) can be express as (Anderson and Haff, 1991):

$$N = \eta(\tau - \tau_t) \quad (8)$$

where τ is the local surface shear stress and τ_t is the threshold shear stress. Obviously, if τ of every position in the computation domain is always smaller than τ_t, no particle can start-up and the drifting snow will not happened. The threshold shear stress can be described as

$$\tau_t = A^2 gd(\rho_p - \rho) \quad (9)$$

in which $A = 0.2$ is more suited to snow as reported by Clifton et al. (2006). The coefficient takes the form of $\eta = C/(8\pi d_p^2)$ (Doorschot and Lehning, 2002) and $C = 1.5$.

The initial velocity of entrained particles follows a lognormal distribution with mean value $3.3u_*$ (u_* is the friction velocity), which is consistent with the measurements of saltating snow in wind tunnel (Nishimura and Hunt, 2000) and has been adopted by drifting snow studies (Clifton and Lehning, 2008; Groot et al., 2014). And the initial take-off angle can be described by a lognormal distribution with a mean value of $(75 - 55(1 - \exp(-\langle d_p \rangle / 1.75 \times 10^{-4})))$ (Clifton and Lehning, 2008).

2.3.2 Rebounding

When a moving particle impact on the bed, it may rebound into air again. If a particle rebounds into the air, it can be described using three variables: the velocity v_{reb}, the angle toward the surface α_{reb} and the angle toward a vertical plane in the streamwise direction β_{reb}.

The rebound probability can be expressed as (Anderson and Haff, 1991):

$$P_{reb} = B[1 - \exp(-\gamma v_{imp})] \tag{10}$$

where v_{imp} is the impact velocity of particle, B and γ are the experienced parameters. Here, $\gamma = 2s/m$ and $B = 0.90$ are employed as Groot et al.(2014) indicate that these value are more accurate for drifting snow.

Recent experiment shows that the fraction of kinetic energy retained by the rebounding particle approximately follows normal distribution (Wang et al., 2008):

$$\mathrm{prob}(v_{reb}^2) = \frac{1}{\sqrt{2\pi}\sigma_{reb}} \exp\left(-\frac{(v_{reb}^2 - \langle v_{reb}^2 \rangle)^2}{2\sigma_{reb}^2} \right) \tag{11}$$

where $\langle v_{reb}^2 \rangle = 0.45 v_{imp}^2$ and $\sigma_{reb} = 0.22 v_{imp}^2$ (Kok and Renno, 2009).

The angle α_{reb} approximately follows an exponential distribution. Although Kok and Renno (2009) suggest the mean value of α_{reb} is 45° and it was used by Groot et al. (2014) for drifting snow, we choose a mean value depending on the mean particle size because many researches indicate that α_{reb} relay on particle size (Rice et al., 1995; Zhou et al., 2006):

$$\left\langle \alpha_{reb} \right\rangle = 161.46 e^{-\frac{d_p}{250\times10^{-6}}} + 0.15 \tag{12}$$

However, the angle β_{reb} was rarely involved in previous studies and may not strongly affect the saltation process (Dupont et al., 2013). Here we choose $\beta_{reb} = 0^\circ \pm 15^\circ$.

2.3.3 Splashing

The newly ejected particles and the ‘dead particles’ (not rebounded) will reach equilibrium when the saltation process becomes stable.

The number of newly ejected particles is usually proportional to the impact velocity and can be written as (Kok and Renno, 2009):

$$N = \frac{a}{\sqrt{gD}} \frac{m_{imp}}{\left\langle m_{ej} \right\rangle} v_{imp} \tag{13}$$

where a is a dimensionless constant in the range of 0.01– 0.05. This value affect the ‘saturation length’ (total transport rate of drifting snow reached equilibrium) to a great extent. We find that $a = 0.03$ is closer to the observation of drifting snow in the wind tunnel (Okaze et al., 2012). While this parameter will not influence the steady state of drifting snow because we found the percentage of eject particles is always less than 3% in the fully developed drifting snow. D is the typical particle size ($\left\langle d_p \right\rangle$ in this paper), m_{imp} is the mass of impacting particle and $\left\langle m_{ej} \right\rangle$ is the average mass of ejection grains.

Once a new particle is splashed into the air, it can also be characterized by its velocity v_{ej}, its angle toward the surface α_{ej} and its angle toward a vertical plane in the streamwise direction β_{ej}.

The speed of the ejected particles is exponentially distributed. Kok and Renno (2009) developed a physical expression of the average dimensionless speed of the ejected particle as follow:

$$\frac{\left\langle v_{ej} \right\rangle}{\sqrt{gD}} = \frac{\left\langle \lambda_{ej} \right\rangle}{a} \left[1 - \exp\left(-\frac{v_{imp}}{40\sqrt{gD}} \right) \right] \tag{14}$$

where $\left\langle \lambda_{ej} \right\rangle$ is the average fraction of impacting momentum applied on the ejecting surface grains. We choose $\left\langle \lambda_{ej} \right\rangle = 0.15$ in this paper, which corresponds to the experimental observation of sand by Rice et al. (1995).

The angle α_{ej} approximately follows an exponential distribution and its mean value is 50° (Kok and Renno, 2009), which was also adopted by Groot et al. (2014) in a small-scale drifting snow simulation. In addition, the angle $\beta_{ej} = 0^{\circ} \pm 15^{\circ}$, similar to Dupont et al. (2013).

2.4 Simulation Details

In this paper we have performed some wind tunnel experiments to obtain the initialization data for the simulation as well as to compare the simulated results with experiment results. The computational region is set as $16m \times 1.0m \times 1.5m$ and divided into two sections, as show in figure 1. The first zone extending from $x = 0m$ to $x = 5m$ is used to develop a turbulent wind field and provide a steady turbulent boundary layer. In this simulation, the turbulent characteristics separating from our wind tunnel results are added on the initial logarithmic velocity profile at beginning and the inlet velocity of fluid will be equal to the wind velocity at the location of $x = 5m$ after 5 seconds, which realizes a long distance development of the turbulent boundary layer. The second zone is the blowing snow region from $x = 6m$ to $x = 16m$, where a loose snow layer is set on the ground.

In this model, the grid has a uniform size of $\Delta x = \Delta y = 0.05m$ in the horizontal direction, and the average mesh size of $\Delta z = 0.03m$ in the vertical direction. The grid is stretched by cubic function to acquire detailed information of the surface layer and the smallest grid is $\Delta z_{min} = 0.002m$.

The actual computation time is 30 seconds, in which the first 10s and the second 10s are respectively used for the development of turbulent boundary layer and the drifting snow, and the last 10s for data statistics. The dynamic Smagorinsky-Germano subgrid-scale (SGS) model is used in this simulation. For the flow field, we apply the rigid ground boundary condition at the bottom, the open radiation boundary in the top, the periodic boundary condition in the spanwise direction, the open radiation boundary condition at the end of the domain along the streamwise direction. The forced boundary is applied in the inflow as mentioned above. Additionally, the snow particles have circulatory motion in the lateral boundary and they will disappear when moving out of the outlet in the end of the domain.

The size distribution of snow particles in the air in this paper is fitted to the experiment results obtained from field observations of SPC (Schmidt, 1984), that is

$$f(d_p) = \frac{d_p^{(\alpha-1)}}{\beta^{\alpha}\Gamma(\alpha)}\exp(-d_p / \beta) \tag{15}$$

where α and β are the shape and scale parameters of gamma-function distribution and we choose a value of 4.65 and 75.27, respectively. Every new ejection or entrainment particle will be given a random size from above distribution and will be tracked separately. The sizes of snow particles in the air are stochastically collected and the size distribution is presented in figure 2. The mean diameter is about $\langle d_p \rangle = 350\mu m$. The results are in consistence with those observational results of the natural snow (Omiya et al., 2011).

The density of snow particles and air are $912kg / m^3$ and $1.225kg / m^3$, respectively. And the surface roughness and the molecular kinematic viscosity of snow particles are $z_0 = \langle d_p \rangle / 30$ and $\nu = 1.5\times 10^{-5}$, respectively.

The processes of snow blowing with the friction wind velocity of $u_* = 0.179 \sim 0.428\ m / s$ are performed with the environmental temperature of $-10^{\circ}C$ and initial relative humidity of 90%. And we found the lower bound of friction velocity for a drifting snow is approximately 0.18 m / s for this situation.

3 Model validations

The wind profile is firstly obtained by the time averaging and spatial averaging of a time-series of wind velocities ($t = 5 \sim 10s$ and the time interval is $0.01s$). As shown in figure 3, the method leads to similar wind profiles to that of wind tunnel experiment at different wind speeds.

Snow transport rate (STR) is one of the most important indicators of the strength of the drifting snow. Figure 4(a) shows the evolution of STR per width along streamwise in different friction wind velocity. It can be seen that the STR per width increases along with the streamwise and gradually reaches a steady state, which is basically consistent with the observation in the wind tunnel by Okaze et al. (2012). And it appears that the distance needed to reach the state is increase with the increasing of friction wind speed. The STR per width (averaging from $x = 14m$ to $x = 15m$) versus friction velocity is presented in figure 4(b). It can be observed that the STR per width increases with friction wind velocity increasing. The relationship of STR per width Q and friction velocity u_* can be expressed as

$$Q = 1.94 u_*^{4.51}$$

which is consistent with the experiment results of Sugiura et al. (1998) and the simulation results of Nemoto and Nishimura (2004).

Then, figure 5 shows the relationship of STR per unit area to the saltation height. As shown in figure 5, the variations in the STR per unit area with height at different friction wind speeds are equivalent, that is, the STR per unit area decreases with height increasing. The comparison of the simulation and experiment results of Sugiura et al. (1998) is also displayed in the inset map of figure 5 and they are in a good agreement.

Subsequently, the velocity distribution of snow particles in the air is shown in figure 6, in which (a) is the average velocity of snow particles along the streamwise direction as a function of height and (b) displays the corresponding velocity probability distribution of snow particles. It can be observed from figure 6(a) that the average velocity of snow particles along the streamwise direction increases with the height increasing, in which the experiment data has been calibrated by wind speed. Good accordance with the experimental results until below 0.02m mainly because mid-air collision near bed surface is high frequency and loses energy.

It can be seen from figure 6(b) that the probability distribution of snow particles' velocity along the streamwise direction obeys the unimodal distribution. In other words, it distributes mainly at $0 \sim 4\,m/s$ and the amount of snow particles moving in the opposite direction is basically less than 3% of the total snow particles. Meanwhile, the probability distribution basically does not change with the friction wind speed, in agreement with our experiment. It should be noted that the high-speed particles in this simulation are significantly more than those captured in the experiments (figure 6(b)). This is mainly because the mean velocity of snow particles increases with height increasing, our measurement is mainly set at lower positions due to the limitation of instrument and thus part of high-speed particles are not being captured.

A more detailed statistics of the percentages of particles that moving at different velocities are showed in figure 6(c). The field observation of Greeley et al. (1996) showing that the proportions of saltating sand particles with velocity smaller than $1.5m/s$ and greater than $4\,m/s$ are greater than 59% and smaller than 3%, respectively. However, the proportion of snow particles with the velocity smaller than $1.5m/s$ is in general smaller than 48% and the percentage of particles with velocity greater than $4\,m/s$ increase with the increasing friction velocity. It can be found that the drifting snow has more high-speed particles than saltating sand, which is mainly because the density of snow particles are significant smaller than sand and they are more easily suspended and followed.

Finally, figure 7 shows the mean size of snow particles along height in the air at different friction velocities and compared with the experimental result of Gromke et al. (2014). All the data have been normalized to the average diameter of overall snow particles. It is clearly that the mean diameter of snow particles in the saltation layer slightly decreases with the height increasing, which is also consistent with the observation of previous works (Nishimura and Nemoto, 2005). However, it appears that the mean diameter increase with increasing height above the saltation layer. The main reason may be that the small particle trends to carry smaller inject velocity, while the larger particle is just the opposite due to the stronger inertia. The rebound velocity is proportional to the incident velocity and thus larger snow particle will rebound with a bigger initial velocity.

4 Results and discussions

4.1 The interaction between turbulent and particle motion

Almost all the flows at atmospheric boundary layer are turbulent. The turbulent fluctuations will affect the movement of snow particles and the particle motion will influence the development of turbulent.

Figure 8 shows the cloud map of velocity along the streamwise direction ($u_* = 0.428\,m/s$) (a) before the snow particles take off (t=10s) and (b) when the drifting snow has been sufficiently developed (t=25s). The slice displays the velocity cloud map of U-direction at height $H = 0.001\,m$. Figures 8(a-1) and 8(a-2) show the contour surface map ($\pm 0.5\,m/s$) of wind velocity along spanwise direction and vertical direction, respectively, at time $t = 10s$, and figures 8(b-1) and 8(b-2) show the corresponding results at time $t = 25\,s$. At the same time, the typical trajectories of snow particles are represented in figure 9, in which the diameter of (a) and (b) are 100 μm and 300 μm, respectively. The blue dotted line denotes the motion trajectory that is not affected by the turbulence and it is calculated by another drifting snow model (Zhang and Huang, 2008) with the same take-off velocity and wind profile.

It can be seen from figure 9 that turbulence can significantly affect the trajectories of snow particles with diameter smaller than 100 μm, and may drive these snow particles moving up to 5~6 *m* during one saltation process. By contrast, the trajectories of larger snow particles are less affected by the turbulent fluctuation. These results are consistent with that of the sand saltation in the turbulent boundary layer performed by Dupont et al. (2013). On the other hand, we can be seen from figure 10 that the wind velocity is significantly decreased in the drifting snow region due to the reaction force of the snow particles, while the TKEs are obviously enhanced during snow drifting. This result is attributed to the fact that velocity gradient is obviously changed when the drifting snow formed (Okaze et al., 2012).

4.2 The formation of snow streamers

The saltation process, either in the field or in the wind tunnel, exhibits a temporospatial discontinuity. This discontinuity is affected by many factors such as turbulent fluctuation, topography, surface moisture, roughness elements, etc (Stout and Zobeck, 1997; Durán et al., 2011). Most previous models are unable to clearly describe the drifting snow structure. The motion trajectory of every snow particle is calculated and further the overall structure of snow saltation layers could be intuitively demonstrated because it describes the macroscopic performance of a large amount of saltating particles.

It can be observed from Figure 11 that snow streamers with high saltating particle concentration obviously swing forward along the downwind direction, merging or bifurcating during the movement. It can also be found that the snow streamers with elongated shape differ greatly in length, but only 0.1~0.2 *m* in width. From the corresponding slices of wind velocity cloud map, it can be seen that many low-speed streaks exist in the near-wall region of the turbulent boundary layer. By comparing the concentration and corresponding velocity cloud map, it is hard to decide the relationship between particle concentration and local wind velocity, which is just like the sand streamers reported by Dupont et al. (2013). This may be due to the complex motion of the snow particles and hysteretic change of local wind. However, the shapes of snow streamers are quite different from that of sand streamers. For example, the snow streamers trend to be longer and thinner in the turbulent boundary layer.

The in-homogeneous take off and splash of the snow particles in the turbulent wind field are the main reasons for the formation of snow streamers. The shape and size of streamers largely depend on the flow structure of the turbulent boundary layer. In addition, during the full development of drifting snow, the saltating particles and wind field are in the state of dynamic balance due to the feedback effect of each other. When the number concentration of snow particles at a certain position is high enough, the local wind velocity will be significantly reduced, resulting in a lower splash level. Thus the streamer will gradually weaken or even disappear. In contrast, the local wind speed in the low concentration region will increase, which enhances the splash process, so the snow particles will grow rapidly and form a streamer. Furthermore, the fluctuating velocity may also change the movement direction of snow particles. All the above reasons together cause the serpentine forward of the snow streamers.

4.3 Velocity of snow particles

As one of the most important aspects to evaluate the accuracy of a drifting snow model, the velocity information (especially in the spanwise direction) of snow particles in the air is worthy of attention although it is seldom given in previous models.

Firstly, the spanwise velocity of snow particles in the air is analyzed. As shown in figure 12, (a) is the distribution of the absolute value of spanwise velocity along the elevation and (b) is the corresponding probability distribution. It is observed from figure 12(a) that the mean velocity along spanwise basically increases with the increasing wind speed. This can also be certified from figure 12(b) that the proportion of snow particles in the air with higher spanwise velocity increases with friction velocity increasing. Furthermore, it can be seen that when the friction velocity is small, the absolute value of spanwise velocity decreases with increasing height; while the law is just the opposite for large friction velocity. And the spanwise velocity of snow particles is an order of magnitude less than that of the streamwise in general. The main reason for this is that turbulent fluctuations are fairly minimal when the wind speed is small, and they exert an increasingly stronger with the growing wind speed.Then, the initial take-off speed distributions of snow particles in three directions are acquired due to they are widely used in the numerical model. The probability distributions of lift-off velocity in a fully developed drifting snow field are presented in Figure 13, in which the (a), (b), (c) and (d) show the distributions of streamwise, spanwise, vertical and resultant velocities, respectively. It is clear that all the velocity components obey the unimodal distribution. The vertical lift-off velocity is basically not affected by the friction wind velocity while the initial take-off speed along streamwise and spanwise trend to increase with the increasing wind speed. This provides a reference for use the probability distributions of initial take-off speed.

5 Conclusions

In this study, the3-D drifting snow process with mixed particle size in the turbulent boundary layer is performed and we conclude that:

(1) Turbulent fluctuation may significantly affect the trajectory of small snow particles with equivalent diameter $d_p \leq 100\ \mu m$, while has little influence on that of particles with larger size. And the saltating particles can strengthen the TKE in the turbulent boundary layer.

(2) Fully developed drifting snow swings forward toward the downwind in the form of snow streamers and the wind velocity is proportional to the concentration of snow particles at different locations of the turbulent boundary layer.

(3) The change of spanwise velocities of snow particles along height relies on the friction velocity and the spanwise velocity is one order of magnitude less than the streamwise direction in general.

Acknowledgements. This work is supported by the State Key Program of National Natural Science Foundation of China (91325203), the National Natural Science Foundation of China (11172118, 41371034), and the Innovative Research Groups of the National Natural Science Foundation of China (11121202), National Key Technologies R & D Program of China (2013BAC07B01).

References

Anderson, R. S., and Haff, P. K.: Wind modification and bed response during saltation of sand in air, Acta Mech., 1, 21-51, 1991.

Bavay, M., Lehning, M., Jonas, T., and Lowe, H.: Simulations of future snow cover and discharge in Alpine head water catchments, Hydrological Processes, 23(1), 95-108, 2009.

Bintanja, R.: Snowdrift suspension and atmospheric turbulence. Part I: Theoretical background and model description, Boundary-Layer Meteorology, 95(3), 343-368, 2000a.

Bintanja, R.: Snowdrift suspension and atmospheric turbulence. Part II: Results of Model Simulations, Boundary-Layer Meteorology, 95(3), 369-395, 2000b.

Clift, R., Grace, J. R., and Weber, M. E.: Bubbles, Drops and Particles, Academic, New York, 1978.

Clifton, A, Rüedi, J-D., and Lehning, M.: Snow saltation threshold measurements in a drifting snow wind tunnel, J. Glaciol., 39, 585-596, 2006.

Clifton, A., and Lehning, M.: Improvement and validation of a snow saltation model using wind tunnel measurements, Earth. Surf. Process. Landforms, 33(14), 2156-2173, doi:10.1002/esp.1673, 2008.

Déry, S., and Yau, M. K.: A Bulk Blowing Snow Model Boundary-Layer, Meteorology, 93(2), 237-251, 1999.

Doorschot, J. J. J., Lehning, M.: Equilibrium saltation: mass fluxes, aerodynamic entrainment, and dependence on grain properties, Boundary-Layer Meteorol., 104(1), 111-130, 2002.

Dupont, S., Bergametti, G., Marticorena, B., and Simoëns, S.: Modeling saltation intermittency, J. Geophys. Res., 118(13), 7109-7128, 2013.

Durán, O., Claudin, P., and Andreotti, B.: On aeolian transport: Grain-scale interactions, dynamical mechanisms and scaling laws Aeolian Research, 3(3), 243-270, 2011.

Fukushima, Y., Etoh, T., Ishiguro, S., Kosugi, K., and Sato, T.: Fluid dynamic analysis of snow drift using a non-Boussinesq k-ε turbulence model (in Japanese with English abstract), Seppyo, 63, 373-383, 2001.

Fukushima, Y., Fujita, K., Suzuki, T., Kosugi, K., and Sato, T.: Flow analysis of developing snowdrifts using a k-ε turbulence model (in Japanese with English abstract), Seppyo, 61, 285-296, 1999.

Gallée, H., Trouvilliez, A., Agosta, C., Genthon, C., Favier, V., and Naaim-Bouvet, F.: Transport of Snow by the Wind: A Comparison Between Observations in Adélie Land, Antarctica, and Simulations Made with the Regional Climate Model MAR, Boundary-Layer Meteorol., 146,133-147, DOI 10.1007/s10546-012-9764-z, 2013.

Gauer, P.: Numerical modeling of blowing and drifting snow in Alpine terrain, J. Glaciol., 47(156), 97-110, doi: 10.3189/172756501781832476, 2001.

Greeley, R., Blumberg, D. G., and Williams, S. H.: Field measurements of the flux and speed of wind-blown sand, Sedimentology, 43(1), 41-52, 1996.

Gromke, C., Horender, S., Walter, B., and Lehning, M.: Snow particle characteristics in the saltation layer, Journal of Glaciology, 60, 431-439, 2014.

Groot Zwaaftink, C. D., Diebold, M., Horender, S., Overney, J., Lieberherr, G., Parlange M., and Lehning, M.: Modelling small-scale drifting snow with a

Lagrangian stochastic model based on large-eddy simulations, Bound. Layer Meteorol., 153, 117-139, DOI:10.1007/s10546-014-9934-2, 2014.

Kok, J. F., and Renno, N. O.: A comprehensive numerical model of steady state saltation (COMSALT), J. Geophys. Res., 114(D17), D17204, 2009.

Mann, G. W., Anderson, P. S., and Mobbs, S. D.: Profile measurements of blowing snow at Halley, Antarctica, J. Geophys. Res., 105, 24491-24508, 2000.

Michaux, J. L., Naaim-Bouvet, F., and Naaim, M.: Drifting-snow studies over an instrumented mountainous site: II. Measurements and numerical model at small scale, Annals of Glaciology, 32(1), 175-181, 2001.

Nemoto, M., and Nishimura, K.: Numerical simulation of snow saltation and suspension in a turbulent boundary layer, J. Geophys. Res., 109, D18206, 2004.

Nishimura, K, Hunt, J. C. R.: Saltation and incipient suspension above a flat particle bed below a turbulent boundary layer, J. Fluid Mech., 417, 77-102, 2000.

Nishimura, K., and Nemoto, M.: Blowing snow at Mizuho station, Antarctica, Phil. Trans. R. Soc. A, 2005, 363, doi: 10.1098/rsta.2005.1599, 2005.

Nishimura, K., Yokoyama, C., Ito, Y., Nemoto, M., Naaim-Bouvet, F., Bellot, H., and Fujita, K.: Snow particle speeds in drifting snow, J. Geophys. Res. Atmos., 119(16), 9901-9913, doi:10.1002/2014JD021686, 2014.

Sugiura, K., Nishimura, K., Maeno, N., and Kimura, T.: Measurements of snow mass flux and transport rate at different particle diameters in drifting snow, Cold Regions Science and Technology, 27(2), 83-89, doi.org/10.1016/S0165-232X(98)00002-0, 1998.

Omiya, S., Sato, A., Kosugi, K., and Mochizuki, S.: Estimation of the electrostatic charge of individual blowing-snow particles by wind tunnel experiment, Annals of Glaciology, 52(58), 148-152, 2011.

Okaze, T., Mochida, A., Tominaga, Y., Nemoto, M., Sato, T., Sasaki, Y., and Ichinohe, K.: Wind tunnel investigation of drifting snow development in a boundary layer, J. Wind Eng. Ind. Aerodyn., 104(106), 532-539, 2012.

Pomeroy, J. W., Gray, D. M., and Landine, P. G.: The Prairie Blowing Snow Model: characteristics, validation, operation, Journal of Hydrology, 144(1-4), 165-192, 1993.

Rice, M. A., Willetts, B. B., and McEwan, I. K.: An experimental study of multiple grain-size ejection produced by collisions of saltating grains with a flat bed, Sedimentology, 42(4), 695-706, 1995.

Schneiderbauer, S., Prokop, A.: The atmospheric snow-transport model: SnowDrift3D, Journal of Glaciology, 52(203), 526-542, 2011.

Stout, J. E., and Zobeck, T. M.: Intermittent saltation, Sedimentology, 44(5), 959-970, 1997.

Sugiura, K., Nishimura, K., Maeno, N., Kimura, T., Measurements of snow mass flux and transport rate at different particle diameters in drifting snow, Cold Regions Science and Technology, 27(2), 83-89, 1998.

Taylor, P.: The Thermodynamic Effects of Sublimating, Blowing Snow in the Atmospheric Boundary Layer, Boundary-Layer Meteorology, 89(2), 251-283, 1998.

Tominaga, Y., Okaze, T., Mochida, A., Sasaki, Y., Nemoto, M., and Sato, T.: PIV measurements of saltating snow particle velocity in a boundary layer developed in a wind tunnel, Journal of Visualization, 16(2), 95-98, 2013.

Uematsu, T., Nakata, T., Takeuchi, K., Arisawa, Y., and Kaneda, Y.: Three-dimensional numerical simulation of snowdrift, Cold Regions Science and Technology, 20(1), 65-73, 1991.

Vinkovic, I., Aguirre, C., Ayrault, M. and Simoëns, S.: Large-eddy Simulation of the Dispersion of Solid Particles in a Turbulent Boundary Layer, Boundary-Layer Meteorology, 121(2), 283-311, 2006.

Vionnet, V., Martin, E., Masson, V., Guyomarc'h, G., Naaim-Bouvet, F., Prokop, A., Durand, Y., and Lac, C.: Simulation of wind-induced snow transport and sublimation in alpine terrain using a fully coupled snowpack/atmosphere model, The Cryosphere, 8, 395-415, doi:10.5194/tc-8-395-2014, 2014.

Wang, D., Wang, Y., Yang, B., and Zhang, W.: Statistical analysis of sand grain/bed collision process recorded by high-speed digital camera, Sedimentology, 55(2), 461-470, doi:10.1111/j.1365-3091.2007.00909.x., 2008.

Xiao, J., Bintanja, R., Déry, S., Mann, G., and Taylor, P.: An intercomparison among four models of blowing snow Boundary-Layer Meteorology, 97(1), 109-135, 2000.

Yamamoto, Y., Potthoff, M., Tanaka, T., Kajishima, T., and Tsuji, Y.: Large-eddy simulation of turbulent gas–particle flow in a vertical channel: effect of considering inter-particle collisions, Journal of Fluid Mechanics, 442, 303-334,

2001.
Zhang, J., and Huang, N.: Simulation of Snow Drift and the Effects of Snow Particles on Wind, Modeling and Simulation in Engineering, 408075-408076, 2008.
Zhou, Y. H., Li, W. Q., and Zheng, X. J.: Particle dynamics method simulations of stochastic collisions of sandy grain bed with mixed size in aeolian sand saltation, J. Geophys. Res., 111(D15), D15108, 2006.

Figures:

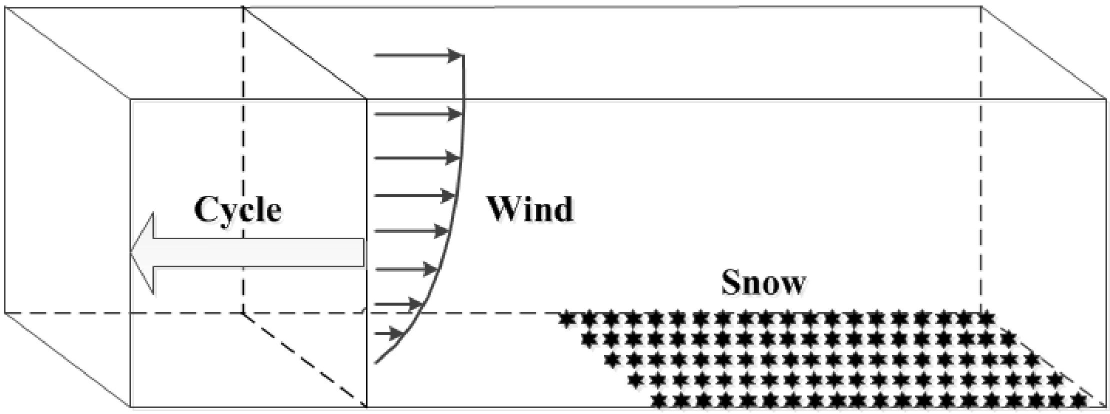

Figure 1. Diagram of computational region.

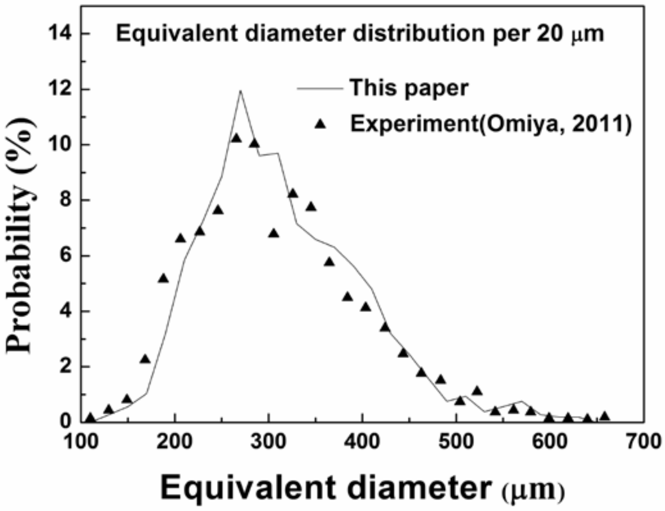

Figure 2. Equivalent diameter probability distribution of snow particles.

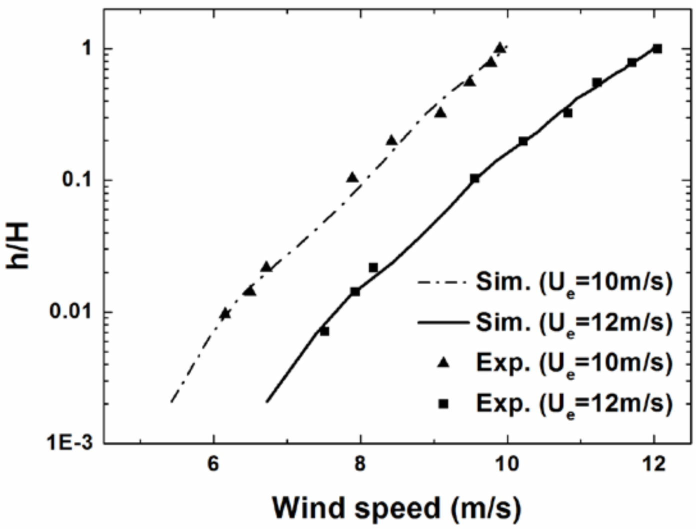

Figure 3. The wind profile at (a) U_e=10m/s and (b) U_e=12m/s.

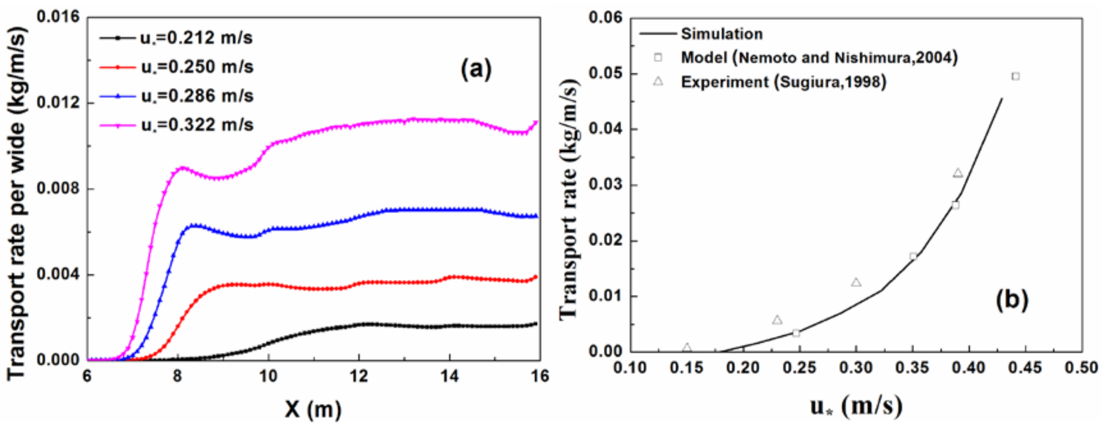

Figure 4. Variation of the snow transport rate (STR) per width with (a) development distance and (b) friction wind velocity.

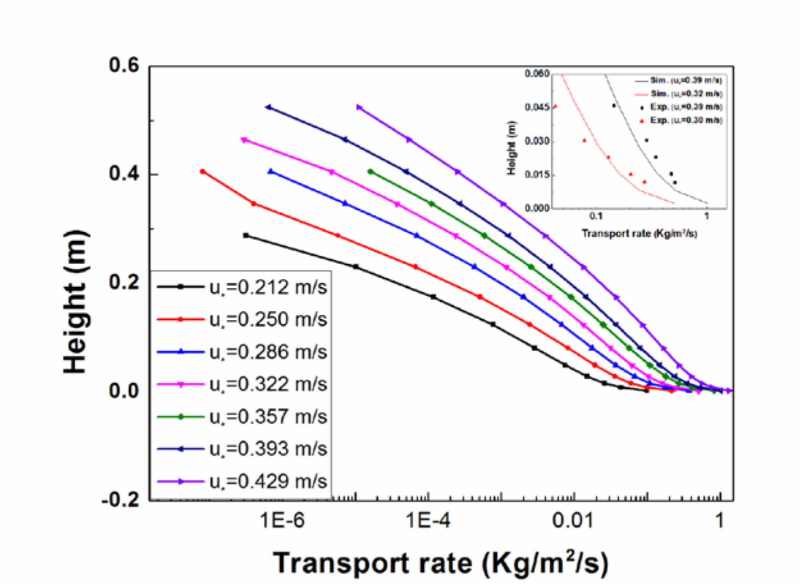

Figure 5. The STR per unit area versus height at different friction wind velocities.

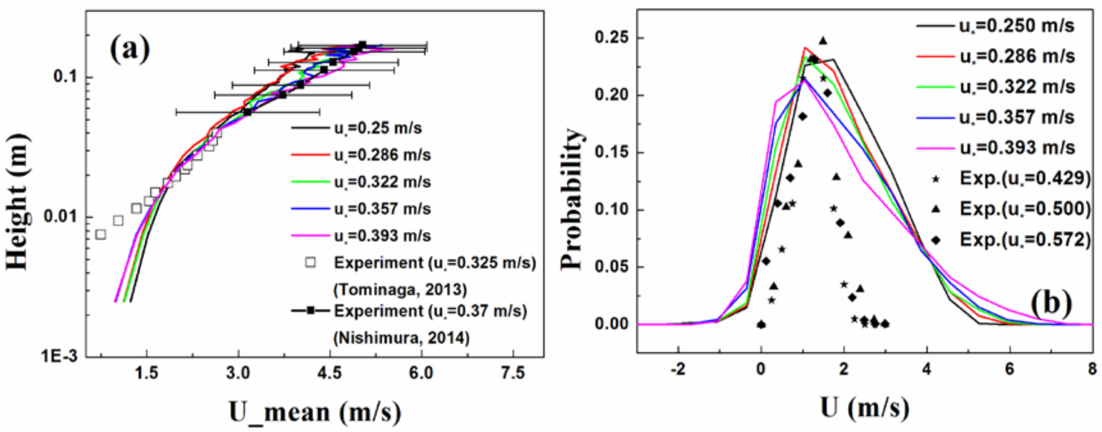

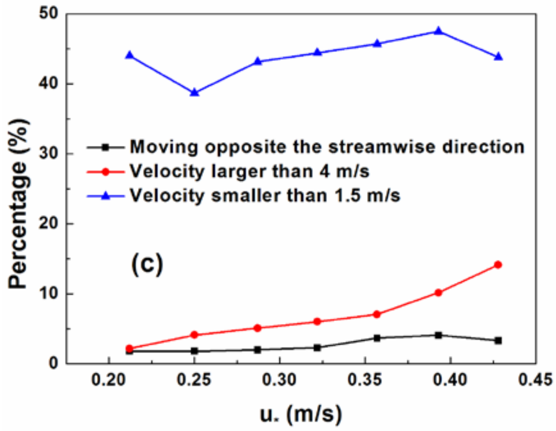

Figure 6. (a)Variation of the average velocity of snow particles along streamwise direction as a function of height, (b) the velocity probability distribution of snow particles and (c) the percentage of particles in different velocity vs friction wind velocities.

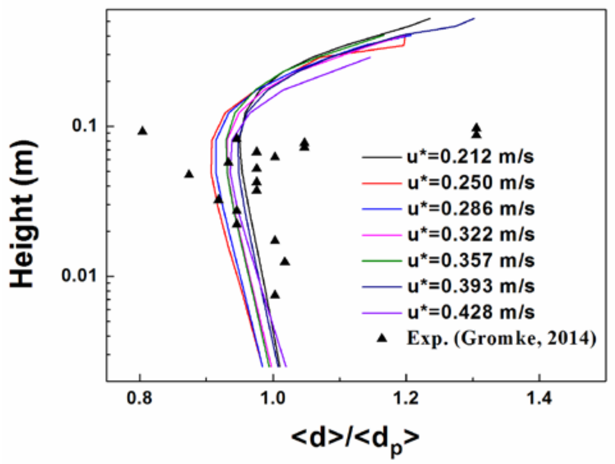

Figure 7. The mean equivalent diameter distribution of snow particles in the air vs height.

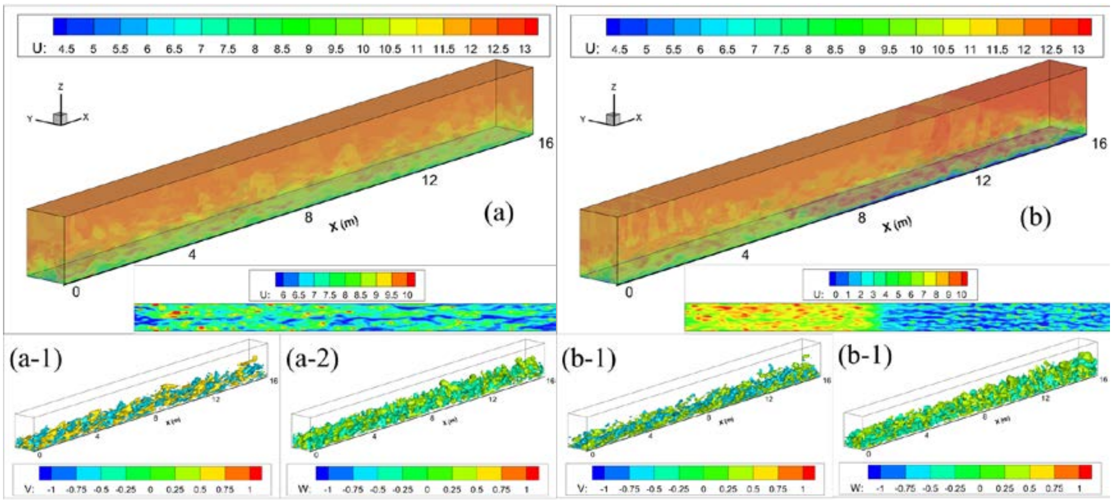

Figure 8. The cloud map of flow field at (a) t=10s and (b) t=25s.

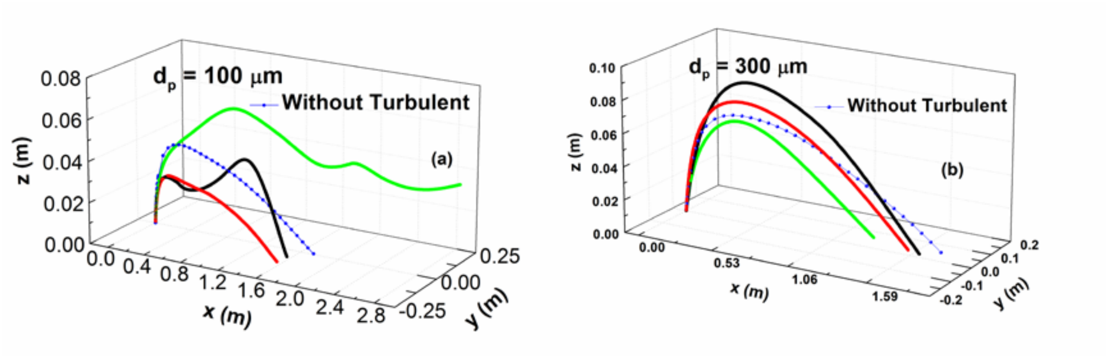

Figure 9. The 3-D trajectories schematic diagram of snow particles with different diameters.

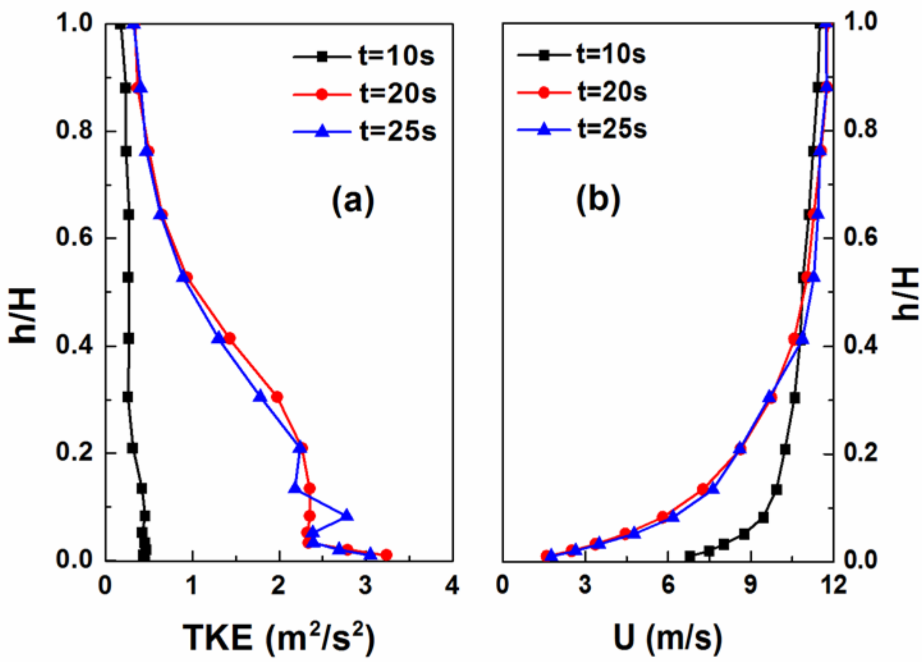

Figure 10. The TKE profile (a) and wind profile (b) at different time, in which the wind data between 13~15m along the downstream is used ($u_* = 0.428\, m/s$).

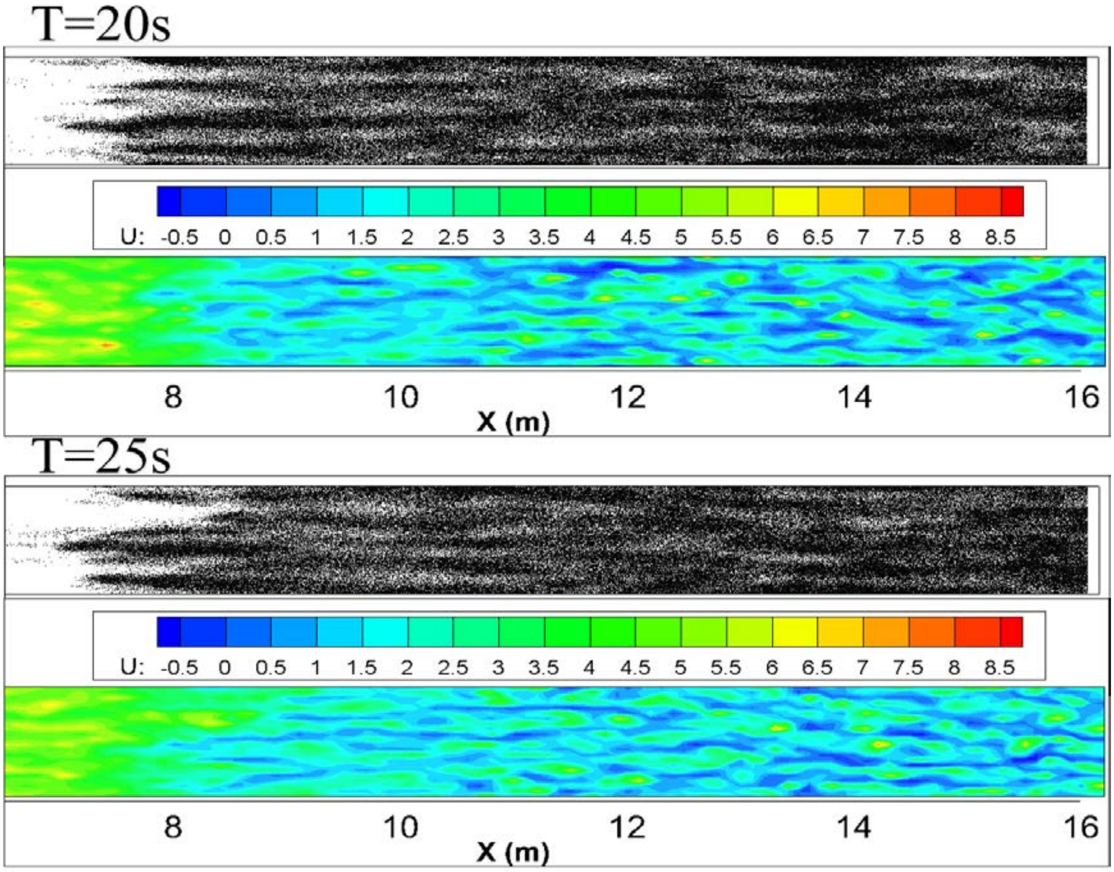

Figure 11. The top view of the particle concentration and the horizontal section of wind velocity cloud map at corresponding moment ($u_* = 0.357\, m/s$, one dark spot stands for a snow particle and the height of horizontal section is $H = 0.001\, m$).

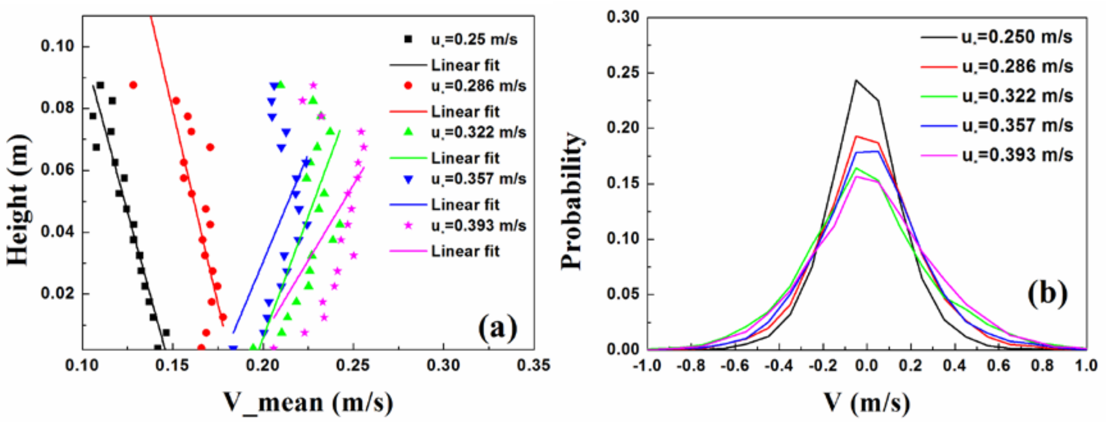

Figure 12. Distribution of (a) the absolute value of spanwise velocity along the elevation and (b) the corresponding probability distribution of snow particles in the air.

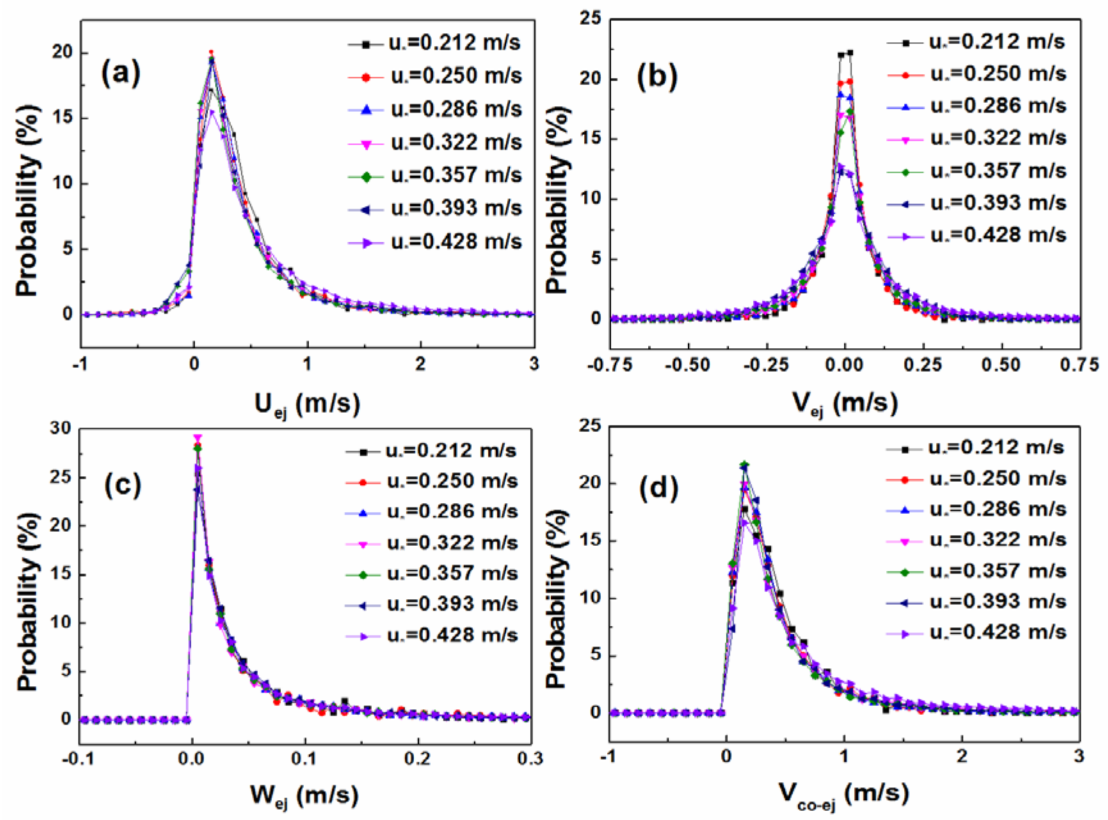

Figure 13. Distribution of the initial (a) streamwise, (b) spanwise, (c) vertical directions and (d) resultant take-off velocity of snow particles.